Polymer Bulletin (2019) 76:3073–3092
https://doi.org/10.1007/s00289-018-2524-6

ORIGINAL PAPER

Synthesis and characterization of stimuli-responsive hydrogel based on starch and methyl-3-aminocrotonate: swelling and degradation kinetics

Muhammad Aslam Malana[1] · Faryal Aftab[1] · Syeda Rabia Batool[1]

Received: 23 February 2018 / Revised: 9 September 2018 / Accepted: 11 September 2018 /
Published online: 26 September 2018

Abstract

Focus of the present studies was to synthesize a novel pH sensitive and thermoresponsive hydrogel which may show swelling behavior suitable for drug delivery at colon part of body. For this purpose, starch was copolymerized with methyl-3-aminocrotonate through free radical polymerization. The structural and thermal characterization of wheat starch/methyl-3-aminocrotonate hydrogel was carried out by XRD, FTIR and TGA. FTIR and XRD confirmed successful formation of the gel. Thermal data were further subjected to the isoconversional method for the determination of kinetic triplet (activation energy E_a, frequency factor A and $g(\alpha)$ function) to predict mechanism for thermal degradation of the synthesized gel. The first step showed a complex mechanism of thermal degradation, i.e., A_2 followed by $A_{3/2}$. Thermodynamic parameters ΔS^* and ΔG^* were also calculated. Moreover, swelling investigations unveiled these gels to be pH sensitive and thermoresponsive. The swelling percentage markedly increased with increasing pH and temperature. Kinetic order of swelling, diffusion mechanism and network parameters (i.e., molecular weight between cross-links and volume faction of polymers) of the synthesized hydrogel was also determined.

Keywords Swelling kinetics · Starch-based hydrogels · Isoconversional method · Stimuli-responsive hydrogel · Methyl-3-aminocrotonate

Introduction

Hydrogels are the hydrophilic polymers that can imbibe large volumes of water or other solvents in their three-dimensional networks. Their elastic behavior and property to swell upon interaction with water or other solutions make them mimic to

✉ Muhammad Aslam Malana
draslammalana@gmail.com

[1] Institute of Chemical Sciences, Bahauddin Zakariya University, Multan 60800, Pakistan

living tissues [1]. The hydrogels can respond to experimental variations in external pH, temperature, ionic strength and solvent type, etc. Because of these distinctive properties, hydrogels have been exploited in biomedical applications such as drug and hormone delivery carriers, wound dressings, tissue engineering of bones [2]. Other practical applications of hydrogels lie in agriculture (fertilizer carriers) [3], industries (paper and textile industries) [4] and catalysis [5], etc.

An immense increase in pollution (due to rapidly growing urge for plastic and pharmaceutical industries) demands a rapid development of strategies which utilize biodegradable materials. Therefore, the use of natural biopolymers, i.e., nontoxic, biodegradable, renewable and abundant in nature, as precursors for the preparation of hydrogels is more promising approach [6]. Starch being one of such biodegradable natural polymers additionally has great cross-linking ability due to abundant –OH groups and hence is considered appreciable precursor for the hydrogel synthesis.

In its native form, starch does not have appreciable thermal and mechanical stability and is hydrophilic that limits its sustainability. Therefore, in order to enhance its mechanical properties, various synthetic monomers, e.g., poly (lactic acid) (PLA), poly (vinyl alcohol) (PVA) and poly (caprolactone) (PCL) have been blended with the starch [6]. The blended polymers sometimes may not exhibit desirable characteristics owing to their poor adhesive interactions. Hence, the synthesis of the cross-linked polymers is a preferable choice. Different cross-linkers used for the cross-linking of starch include phosphoryl chloride, [7] epichlorohydrin, [8] sodium trimetaphosphate [9] and glutaraldehyde [10]. However, the use of some harmful and non-biodegradable cross-linkers in polymers limits their applications in biomedicine. Hence, need of the day is to synthesize and develop a cross-linked polymer that meets all the above-mentioned essentials. Di(ethyleneglycol) dimethacrylate (DEGDMA) is a biocompatible cross-linking agent that provides stable networks in a wide range of pHs and temperatures under in vitro conditions. Thus, it can generate a useful drug delivery carrier as established earlier [11].

Wheat starch is one of the most commonly available and cheap starches. Its every minute granule consists essentially of linear amylose structure and branched amylopectin structure [12, 13]. Researchers have attempted various copolymers of wheat starch using different hydrophilic monomers, e.g., acrylic acid [14], lactic acid [15] and PVC [16] to enhance its thermal and mechanical stability. However, still some areas of research need to be explored particularly starch grafted with hydrophobic monomers. Methyl-3-aminocrotonate (MAC), a hydrophobic monomer, has pharmaceutical importance as it is used as an intermediate in the synthesis of efficient drugs (e.g., 1, 4-dihydropyridine derivatives [17] and nitrendipine [18]) for treating hypertension and other chronic diseases reflecting biocompatibility of the monomer. Due to its biocompatibility, MAC was selected as a monomer to make its copolymer with wheat starch in these studies. It is expected that MAC, being a bulky monomer, will increase the hydrophobicity of copolymer which will restrict the hydrogel to release the drug easily; thus, the drug can travel to the targeted part of body without affecting other body parts. Keeping in view all this discussion, wheat starch/methyl-3-aminocrotonate (WSCR) was copolymerized through free radical polymerization by using ammonium persulfate as an initiator and DEGDMA as a cross-linker.

Thermal behavior of these polymers is useful to anticipate their stability and proposed applications [19–21]. However, literature reviews few reports of mechanistic details for thermal degradation of starch-based copolymers. In this report, therefore, detailed thermal analysis of the synthesized copolymer was explored. Thermogravimetric analysis was selected as a tool for determination of thermal stability, kinetic and thermodynamic parameters of the copolymer. Moreover, the swelling measurements of the copolymer were also carried out to examine the suitability of the copolymer for drug delivery applications. Fourier transform infrared (FTIR) spectra and X-ray diffraction (XRD) patterns of wheat starch and its copolymer have also been discussed in this manuscript.

Experimental

Materials

Native wheat starch (Sigma-Aldrich, 99%), methyl-3-aminocrotonate (Aldrich, 97%), ethanol (AnalaR, 99%), ammonium persulfate (Fischer scientific, > 98%) and DEGDMA (Aldrich, 95%) were used for the synthesis of WSCR hydrogel.

Synthesis of the hydrogel

Native wheat starch (4.0 g) was diluted in 208.0 ml of deionized water in three necked quick fit flask. This mixture was stirred and heated at 373 K for an hour under nitrogen atmosphere. A condenser was adjusted on the quick fit flask to reflux the reaction mixture. After an hour, the slurry of wheat starch was transformed into an opaque gel-like paste [22]. This paste has some agglomerations which may be due to less soluble part of starch, i.e., amylose. These agglomerations were removed by sieving, and homogenized gel thus obtained was further subjected to polymerization. The monomer, methyl-3-aminocrotonate (4.0 g), was dissolved in ethanol (10 ml) and added to 173.0 g of wheat starch gel. DEGDMA (8 ml) and ammonium persulfate (1% w/w) were used as cross-linking agent and initiator, respectively. The nitrogen gas was bubbled through the reaction mixture to eliminate the interference of oxygen. The assembly was closed and incubated for 72 h at 323 K. The synthesized polymer was separated, washed with ethanol and deionized water to remove the unreacted materials and dried in an electric oven at 333 K for 6 h. The yellowish WSCR co-polymeric hydrogel was reserved for further investigations. The proposed mechanism for synthesis of WSCR hydrogel is shown in Fig. 1.

Fourier transform infrared (FTIR) spectroscopy

The FTIR spectra of wheat starch, methyl-3-aminocrotonate monomer and WSCR hydrogel were recorded using NICOLET 6700 FTIR Spectrophotometer, Thermo Scientific, USA. These spectra were used to identify the functional groups present in the monomers and polymer.

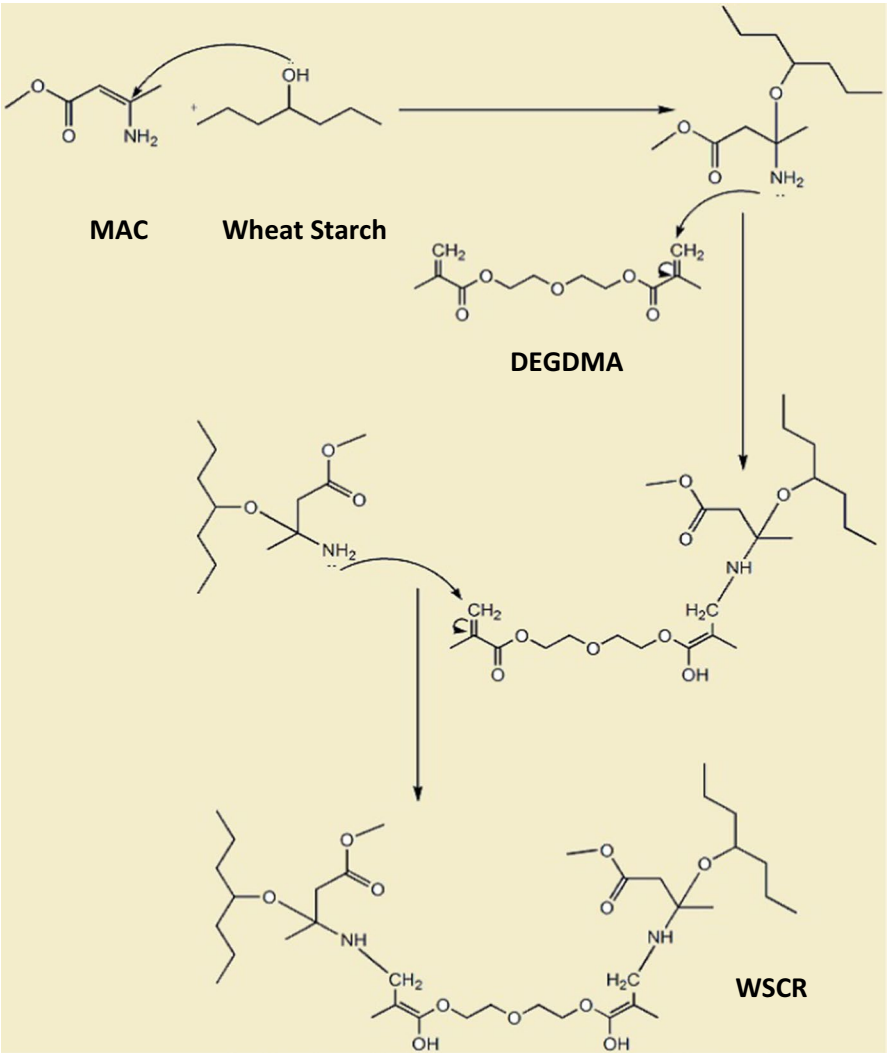

Fig. 1 Proposed scheme for the synthesis of WSCR hydrogel

X-ray diffraction analysis

Wheat starch and WSCR hydrogel were subjected to XRD analysis using PAnalytical X-ray diffractometer. This instrument uses Cu-kα as a radiation source ($\lambda = 1.54$ Å) at a 40 kV generator voltage and 30 mA tube current allowing the scan in 2θ ranging from 10° to 70° with the scan rate of 0.02°/s.

Thermogravimetric analysis

The synthesized WSCR hydrogel was analyzed at three different heating rates (i.e., 10, 15 and 20 K/min) by using Perkin Elmer TG/DTG Diamond instrument. The temperature was raised from ambient to 923 K, and the data obtained were subjected to various kinetic and thermodynamic determinations by isoconversional methods.

Swelling of hydrogel

The powdered WSCR hydrogel was tested for its water retaining behavior at different pH, i.e., 1.0, 3.0, 5.0, 7.0 and 8.0 and at 303 K and 313 K. The gel sample was allowed to uptake water till the swelling equilibrium was achieved. During this process, swollen gel was weighed after different intervals of time.

Results and discussion

Characterization of functional groups by FTIR analysis

The FTIR spectra of wheat starch, monomer and WSCR are shown in Fig. 2.

The IR spectrum of wheat starch showed that C–H stretching was displayed at 2921 cm^{-1}. Furthermore, a broad absorption band for O–H stretching appeared at 3286 cm^{-1} and peaks at 1217 cm^{-1}, 1149 cm^{-1} and 1075 cm^{-1} attributed to C–O– stretching [23]. In case of methyl-3-aminocrotonate, the characteristic peaks at 3411 cm^{-1}, 3314 cm^{-1} and at 1559 cm^{-1} appeared due to $–NH_2$ group. The bands at 1650 cm^{-1} (C=C– stretching) and 1444 cm^{-1}(C–H stretching) were assigned to the unsaturation present in the monomer. The characteristic absorption

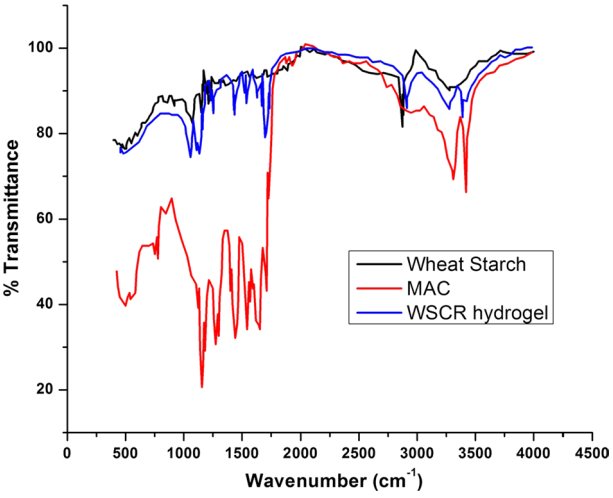

Fig. 2 FTIR spectra of wheat starch, MAC and WSCR hydrogel

peaks of α, β-unsaturated esters appeared at 1288 cm^{-1}, 1185 cm^{-1}, 1162 cm^{-1} (C–O stretching) and 1750 cm^{-1} (C=O stretching, weak). Whereas in the case of WSCR hydrogel, all absorption peaks of wheat starch were present with O–H peak shifted from 3286 to 3275 cm^{-1}, and peak due to C–H stretching was shifted from 2921 to 2895 cm^{-1} (broad peak). In addition to this peak shifting, new bands were registered at 3393 cm^{-1} and 1540 cm^{-1} which were characteristic absorption peaks of $–NH_2$ group attributed to the presence of $–NH_2$ group in grafted polymer structure. Another broadband appeared at 1264 cm^{-1} which was present in MAC (for C–O stretching in α, β-unsaturated esters), whereas the peaks at 1149 cm^{-1} and 1077 cm^{-1}(for C–O stretching in alkanes) were initially present in the starch as well. At 1720 cm^{-1}, there was a characteristic peak due to C=O stretching of α, β-unsaturated esters which was present at 1750 cm^{-1} in MAC. The polymer also exhibited weak absorption peaks at 1652 cm^{-1} and 1456 cm^{-1}, but comparatively sharp absorption bands were present in MAC at these frequencies which ascribed that unsaturation has been reduced in the polymer. It could be possibly assumed that either the neighborhood of unsaturated carbon atom was changed or the unsaturation might have been reduced to some extent. The peak shifting and appearance of new characteristic bands confirmed the formation of WSCR hydrogel and supported the mechanism of chemical reaction for the formation of hydrogel represented in the scheme.

XRD analysis

The powder pattern of native starch and WSCR hydrogel are depicted in Fig. 3. Starches in general show two types of diffraction pattern, i.e., A-type patterns (especially cereals starches) giving peaks at $2\theta = 15°$, 17°, 18°, 20° and 23.5° and the most common B-type patterns with peaks at 2θ angles of 5.6°, 14.1°, 15°, 17°, 19.7°, 22.2° and 24° [24]. Starches are generally semicrystalline in nature showing clear peaks in their XRD pattern due to the presence of amylopectin fraction [25]. In the present case, powder pattern of unmodified wheat starch (Fig. 3a) shows

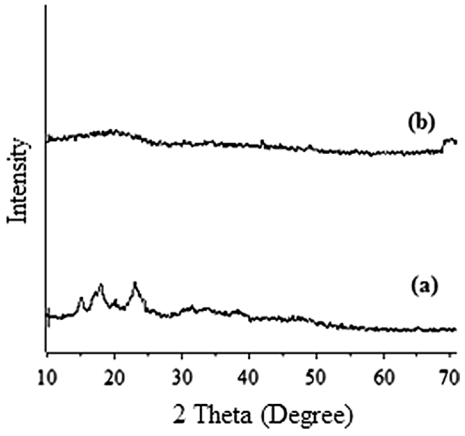

Fig. 3 XRD patterns of (a) wheat starch (b) WSCR hydrogel

a B-type diffraction pattern displaying peaks at $2\theta = 15.0°$, 17.9° and 23.0°. These peaks refer to the presence of crystallinity in starch upheld because of hydrogen bonds and crystalline amylopectin content in its structure. But in the diffraction pattern of WSCR hydrogel (Fig. 3b), the degree of crystallinity has been reduced as a broadband appears from 15° to 25°. This broadness of peaks accounts for drop in crystallinity of starch due to breakage of H-bonds in starch, thus confirming the formation of WSCR gel. This also reflects that in addition to the amorphous content of starch, i.e., amylose the crystalline part (amylopectin) also takes part in copolymerization of starch gel with MAC [25].

Thermal analysis

The TGA curves of WSCR hydrogel at three different heating rates are presented in Fig. 4a. Initially, the weight loss of 9.57% is observed in the temperature range 298–383 K. This may be due to the loss of moisture revealing somewhat hydrophilic character of copolymer, as it absorbs water at very low temperature. Three major degradation steps are evident in the TGA curve (Fig. 4a). In first step, weight loss of 15.69% occurs in the temperature range of 484.2–535.1 K. The temperature corresponding to maximum weight loss in this step ($T_p = 516.2$ K) is close to the decomposition temperature of DEGDMA (i.e. 513.2 K); it is therefore assumed that

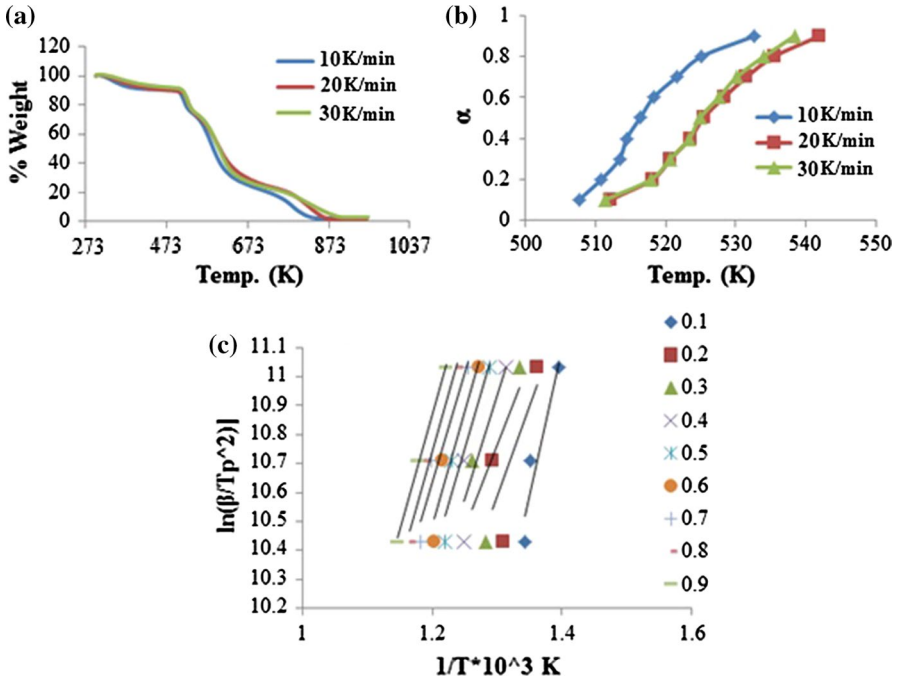

Fig. 4 **a** TGA curve of WSCR hydrogel at different heating rates **b** representative α–T curve for second step (535.6–701.2 K). **c** Representative KAS plot for third step (701.8–841.9 K) to determine E_a

evaporation of DEGDMA takes place in this step. The second step (535.6–701.2 K) with the maximum weight loss of 52.34% may correspond to the breakdown of polymer backbone. The third stage (701.8–841.9 K) with weight loss of 19.86% may be due to the degradation of long chains of wheat starch.

The progress of degradation reaction is generally investigated by α, which is fraction of sample reacted (also known as degree of conversion) at any temperature T and it helps in the determination of reaction rate and is given by the formula:

$$\alpha = \frac{m_o - m_i}{m_o - m_f} \tag{1}$$

where m_o = initial %age weight of sample present, m_f = final %age weight of sample and, m_i = %age weight of sample at the given temperature.

The average activation energy for all steps is calculated by Kissinger method (Eq. 2)

$$\ln \beta/T^2 = \text{const} - yE/RT \tag{2}$$

Here β is the heating rate, and T is the temperature at given degree of conversion [26]. A plot of $\ln(\beta/T^2)$ v/s $1/T$ gives a straight line for each α value whose slope is used for calculation of activation energy, which is 142.93 kJ/mol for first step of thermal degradation of WSCR (Fig. 4c).

There are no consequential variations in α–T curve (Fig. 4b) at different heating rates, in this stage, which recommend similar relationship of temperature with degree of conversion (α) for all heating rates [26].

The reaction mechanism is determined by master plot method (Eq. 3)

$$g(\alpha)/g(0.5) = p(\alpha)/p(x_{0.5}) \tag{3}$$

The theoretical master plots are determined by plotting $g(\alpha)/g(0.5)$ against α. Here, $g(\alpha)$ represents various models, presented in Table 1, which control the degradation process, while $g(0.5)$ is the $g(\alpha)$ value for a reference point $\alpha = 0.5$ [26]. Similarly, the experimental master plots are obtained by plotting $p(x)/p(0.5)$ and α. To solve $p(x)$ in this paper, Senum–Yang fourth degree approximation (Eq. 3a) was used [27].

$$\begin{aligned} p(x) &= \frac{e^{-x}\pi(x)}{x} \\ \pi(x) &= \frac{x^3 + 18x^2 + 86x + 96}{x^4 + 20x^3 + 120x^2 + 240x + 120} \end{aligned} \tag{3a}$$

where $x = E/RT$ and $p(0.5)$ is the $p(x)$ for a reference point when $\alpha = 0.5$.

The theoretical plot for the given $g(\alpha)$ model which matches best with the experimental master plot will actually control the degradation mechanism.

In the present investigations, the reaction mechanism determined by master plot method (Eq. 3) suggests that first stage follows a complex degradation mechanism (A_2 model for $\alpha = 0.1$–0.5 and $A_{3/2}$ model for $\alpha = 0.6$–0.9), depicting initial one-dimensional

Table 1 Several models used to discuss solid-state kinetics [26]

No.	Mechanism code	Function name	$g(\alpha)$ model	Rate controlling mechanism
Chemical reaction mechanism				
1	$F_{1/3}$	1/3rd Order	$1-(1-\alpha)^{2/3}$	Chemical reaction
2	$F_{3/4}$	3/4th Order	$1-(1-\alpha)^{1/4}$	-do-
3	$F_{2/3}$	2/3rd Order	$(1-\alpha)^{1/2}-1$	-do-
4	F_2	2nd Order	$(1-\alpha)^{-1}-1$	-do-
5	F_3	3rd Order	$(1-\alpha)^{-2}-1$	-do-
Acceleratory rate equations				
6	$P_{3/2}$	Maple power law	$\alpha^{3/2}$	Nucleation
7	$P_{1/2}$	Maple power law	$\alpha^{1/2}$	-do-
8	$P_{1/3}$	Maple power law	$\alpha^{1/3}$	-do-
9	$P_{1/4}$	Maple power law	$\alpha^{1/4}$	-do-
Sigmoidal rate equations/random nucleation and subsequent growth				
10	A_1, F_1	Avrami–Erofeev equation	$-\ln(1-\alpha)$	Supposed random nucleation and its growth, $n=1$
11	$A_{3/2}$	Avrami–Erofeev equation	$-\ln(1-\alpha)^{2/3}$	Supposed random nucleation and its growth, $n=1.5$
12	A_2	Avrami–Erofeev equation	$-\ln(1-\alpha)^{1/2}$	Supposed random nucleation and its growth, $n=2$
13	A_3	Avrami–Erofeev equation	$-\ln(1-\alpha)^{1/3}$	Supposed random nucleation and its growth, $n=3$
14	A_4	Avrami–Erofeev equation	$-\ln(1-\alpha)^{1/4}$	Supposed random nucleation and its growth, $n=4$
15	A_u	Prout-Tomkins equation	$\ln[\alpha/(1-\alpha)]$	Branching nuclei
Deceleratory rate equations/phase boundary equations				
16	R_1, F_o, P_1	Power law	A	Contracting disk
17	R_2, $F_{1/2}$	Power law	$1-(1-\alpha)^{1/2}$	Contracting cylinder
18	R_3, $F_{2/3}$	Power law	$1-(1-\alpha)^{1/3}$	Contracting sphere
Equations of diffusion mechanism				
19	D_1	Parabola equation	α^2	One-dimensional diffusion

Table 1 (continued)

No.	Mechanism code	Function name	$g(\alpha)$ model	Rate controlling mechanism
20	D_2	Valensi equation	$\alpha+(1-\alpha)\ln(1-\alpha)$	Two-dimensional diffusion
21	D_3	Jander equation	$[1-(1-\alpha)^{1/3}]^2$	Three-dimensional diffusion, spherical symmetry
22	D_4	Ginstling–Brounstein equation	$1-2\,\alpha/3-(1-\alpha)^{2/3}$	Three-dimensional diffusion, cylindrical symmetry
23	D_5	Zhuravlev, Tempelman equation	$[(1-\alpha)^{-1/3}-1]^2$	Three-dimensional diffusion
24	D_6	Anti-Jander equation	$[(1-\alpha)^{1/3}-1]^2$	-do-
26	D_7	Anti-Ginstling–Brounstein equation	$1+2\alpha/3-(1+\alpha)^{2/3}$	-do-
26	D_8	Anti-Zhuravlev, Lesokhin, Tempelman equation	$[(1+\alpha)^{-1/3}-1]^2$	-do-

random nucleation followed by three-dimensional growth of nuclei (Fig. 5a). Similar complex mechanism has also been reported for understanding the crystallization mechanism of a wallastonite base glass using isoconversional, IKP methods and master plots [17].

In the second step, degradation of WSCR polymer is due to second-order chemical reaction thus following F_2 mechanism (Fig. 5b). The third step can be well described by A_2 mechanism which is indicative of one-dimensional random nucleation (Fig. 5c). For confirming the reaction mechanism, $g(\alpha)$ model for all the steps is reconstructed by using Eq. 3b. The frequency factor A is also determined by slope of the plot of $g(\alpha)$ v/s $E^*p(x)/\beta R$ (Eq. 3b).

$$g(\alpha) = \frac{AE}{R}\int_{x}^{\infty}\frac{\exp(-x)}{x^2}\mathrm{d}x = \frac{AE}{\beta R}p(x) \tag{3b}$$

where $g(\alpha)$ represents different theoretical models presented in Table 1 where $p(x)$ and other terms are defined earlier. All the reconstructed plots confirmed the discussed reaction mechanisms. Representative plot of reconstructed model for second step is shown in Fig. 5d. The values of kinetic triplet, i.e., activation energy E_a, frequency factor A and model of thermal degradation for all stages are presented in Table 2. These values are in good agreement with those calculated from Coats-Redfern method (Eq. 4) and are listed in Table 2 [28].

$$\ln g(\alpha)/T^2 = \ln AR/\beta E - E/RT + \left(1 + 2RT/E\right) \cong \ln AR/\beta E - E/RT \tag{4}$$

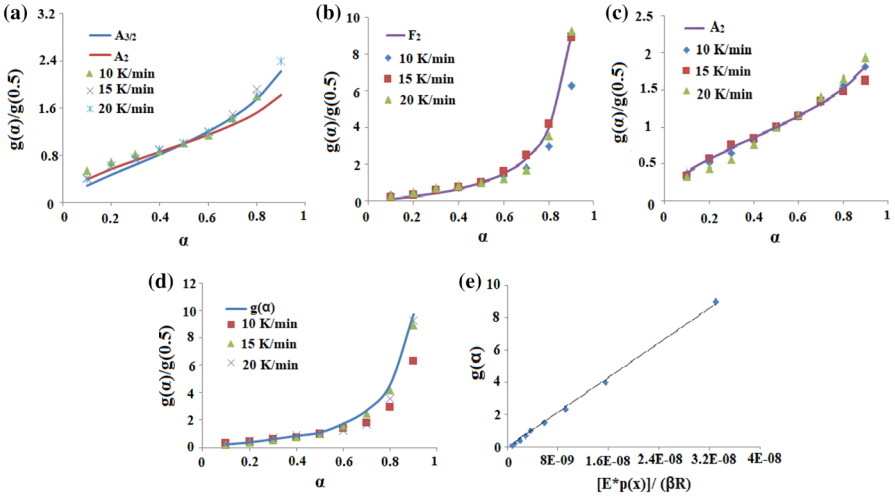

Fig. 5 Experimental and theoretical master plots to determine the kinetic model of WSCR decomposition in **a** first step. **b** Second step. **c** Third step. **d** Reconstructed $g(\alpha)$ model for second step. **e** Representative plot to determine frequency factor A for second step

Table 2 Kinetic triplet obtained from Kissinger and Coats-Redfern method for thermal degradation of WSCR hydrogel

Step	Methods	Activation energy (kJ/mol)	*A* (1/s)	Model
First	Kissinger	142.92782	2×10^{15}	A_2 (assumed random nucleation and its growth $n=2$) $A_{3/2}$ ($n=1.5$)
	Coats-Redfern (15 K/min)	A_2 126.1816	4.46×10^{13}	
		$A_{3/2}$ 171.152	1.89×10^{15}	
Second	Kissinger	86.876958	3.0×10^{8}	F_2 (chemical reaction)
	Coats-Redfern	100.1671	3.20×10^{9}	
Third	Kissinger	63.175315	6.3×10^{4}	A_2 (assumed random nucleation and growth)
	Coats-Redfern	60.42366	2.08×10^{4}	

All the terms in Eq. 4 have same meanings as mentioned above.

The values of A for all the steps are evaluated by using Eq. 3, and representative plot to determine *A* value for second step is shown in Fig. 5e. The values of frequency factor (A) at first and second steps of degradation were 2×10^{15} and 3×10^{8}, respectively. These results may be explained in terms of rotation of reactants and activated complex along the surface. In the former case, i.e., for $A=2\times10^{15}$, it is assumed that activated complex unlike reactants is free to rotate parallel to the surface. Whereas in the later case, activated complex is highly restricted and the reactants rotate freely. This interpretation is in line with the argument given by Vlaev et al. [29] and Bamford et al. [30] while comparing the kinetic results of non-isothermal degradation of calcium oxalate monohydrate.

Thermodynamic parameters

Thermodynamic parameters ΔS^*, $\Delta H^*$and ΔG^* were calculated for thermal degradation of WSCR hydrogel using Eqs. 5, 6 and 7, respectively, and are given in Table 3.

$$\Delta S^* = R \ln \frac{Ah}{e\chi k_B T_P} \tag{5}$$

Table 3 Thermodynamic parameters calculated from Kissinger and Coats-Redfern method for WSCR hydrogel

Step	Methods	ΔS^* (J/Kmol)	ΔH^* (kJ/mol)	ΔG^* (kJ/mol)
First	Kissinger	−832.309	138.624	569.849
	Coats-Redfern (20 K/min)	A_2 −765	A_2 121.82	A_2 522.89
		$A_{3/2}$ −734	$A_{3/2}$ 166.79	$A_{3/2}$ 551.137
Second	Kissinger	−960.9	81.93	655.65
	Coats-Redfern (15 K/min)	−843	95.22	596.93
Third	Kissinger	−1031.03	56.76	852.18
	Coats-Redfern (20 K/min)	−959	40.17	828.38

$$\Delta H^* = E - RT_p \tag{6}$$

$$\Delta G^* = \Delta H^* - T_p \Delta S^* \tag{7}$$

The values of ΔG^*, free energy for the formation of activated complex from reactant precursors, [31] gradually increase from first to third step indicating that as the degradation reaction precedes it becomes more and more non-spontaneous. So, in third step, more energy (high temperature) is required to carry out degradation reaction. ΔH^* indicates the energy difference between the reagents and the activated complex [31]. Generally, the small values of ΔH^* favor the formation of activated complex due to this low potential energy barrier and vice versa. In the presented case, ΔH^* decreases from first to third step which shows that going from first to third step, formation of activated complex becomes easier as potential energy barriers are gradually decreasing. The ΔS^* values obtained are exceptionally low (Table 3) indicating that the activated complex is more arranged than reactants.

Swelling studies of hydrogel

Percentage swelling (S %) of WSCR calculated by using Eq. 8 (Fig. 6a, b) showed that percentage swelling increased with time, until it reached to its limiting value referred to as equilibrium swelling W_e.

$$\%S(m) = \frac{W_t - W_o}{W_o} \times 100 \tag{8}$$

Here W_t is weight of swollen hydrogel at any time t, and W_o is weight of dried hydrogel.

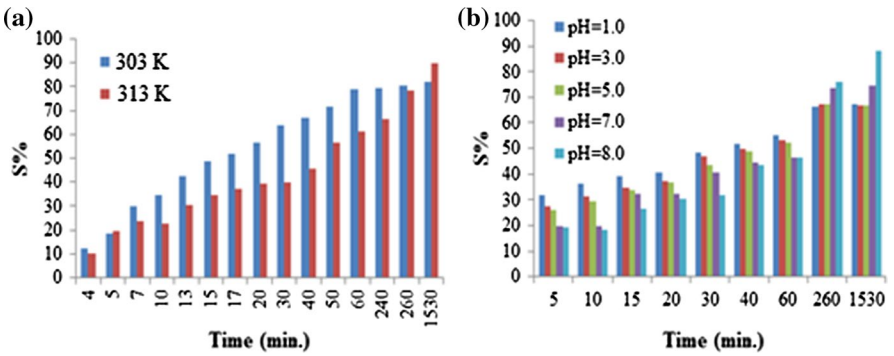

Fig. 6 **a** Effect of temperature on % swelling of WSCR hydrogel, **b** effect of pH on % swelling of WSCR hydrogel

Thermosensitivity of the gel

The curve showing swelling of WSCR hydrogel as a function of time at two different temperatures, i.e., 303 K and 313 K is shown in Fig. 6a. At lower temperature dynamic swelling was greater than that at higher temperature, whereas the trend was reversed in case of equilibrium swelling.

This increase in percent swelling with temperature may be attributed to differential penetration of water into the network structure. At lower temperature, water molecules diffused in bound form into the polymer network, whereas at higher temperature, the molecules gained energy and intermolecular H-bonding between water molecules may break thus facilitating their entry in the hydrogel. Similar interpretations for greater swelling in wheat straw cellulose-based semi-IPNs hydrogel at higher temperature were given by Jia Liu et al. in 2014 [32].

pH sensitivity

Figure 6b shows the swelling response of WSCR hydrogel at pH 1.0, 3.0, 5.0 7.0 and 8.0 at 313 K. It was clear from the figure that dynamic swelling is maximum at pH 1.0. It was assumed that $–NH_2$ group of MAC gets protonated in acidic conditions ($pK_b > pH$). This increased the hydrophilic ability of the gel due to chain relaxation [33]. This is why dynamic swelling in acidic conditions was higher as compared to that in neutral or basic conditions. Furthermore, ionization of carboxymethyl group at pH higher than pKb would cause electrostatic repulsions and chain expansion leading to enhanced equilibrium swelling [34, 35]. So it might be concluded that the swelling behavior of this specific system was strongly controlled by the $–NH_2$: $–COOCH_3$ ratio present in the gel network structure. So in acidic medium, the $–NH_2$ groups were proving to be more effective, whereas $–COOCH_3$ contributes more to the swelling percentage of the gel in basic conditions. The pH sensitivity of the system indicates that this hydrogel may be useful for controlled release of drug inside the body because medium of stomach is acidic while that of intestine has basic pH.

Mechanism of swelling

Before using hydrogels as drug delivery carriers, it was essential to understand diffusion mechanism. The diffusion required the movement of solvent into previously established or thermodynamically formed spaces between the networks of macromolecules resulting into enhanced separations between cross-linked chains [36].

$$\frac{W_t}{W_e} = kt^n \tag{9}$$

In the present work, Eq. 9 is applied on initial stages of solvent penetration to evaluate the mechanism of swelling. In this equation, W_t and W_e correspond to the weight of solvent absorbed at any time t and at equilibrium, respectively. The slope of the graph ln W_t/W_e vs lnt gives the value of constant n (diffusion exponent), and intercept gives the value of k (swelling rate constant) [37]. Mechanism of swelling of polymer could

be inferred from the values of diffusion exponent (n). It has been suggested that if value of n is between 0.45 and 0.5 the diffusion of the medium into the hydrogel followed Fickian mechanism and if n was greater than 0.5 and less than 1 the mechanism of diffusion was non-Fickian (i.e., transport is primarily due to chain relaxation of polymer as well as diffusion of solvent) [38].

Representative plots for the determination of diffusion exponent n at different temperatures (303 and 313 K) and pH (8.0) are shown in Fig. 7a, b, respectively. As far as the swelling mechanism of the gel under discussion is concerned, it was found that diffusion of water into polymer network showed anomalous behavior ($0.5 < n < 1$) at all pH values at 313 K, whereas mixed behavior was observed at 303 K (Table 4). It suggested that process of swelling of WSCR hydrogel was controlled by diffusion and chain relaxation at higher temperature. At lower values of temperature and pH, process of swelling was found to be diffusion controlled only but at higher pH it was also controlled by chain relaxation.

Kinetic order of swelling

In order to determine kinetic order of swelling of WSCR hydrogel, pseudo-first order (Fick's model) and pseudo-second order (Schott model) expressed by Eqs. 10 and 11, respectively, were applied to the experimental data.

$$\ln \frac{W_e - W_t}{W_e} = -kt \tag{10}$$

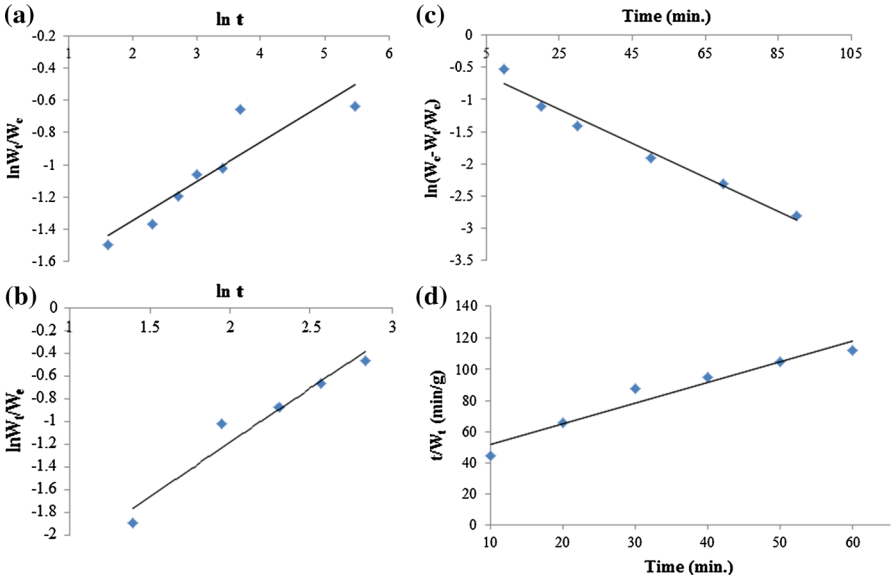

Fig. 7 Representative plots for the determination of diffusion exponent at **a** pH 8.0, 303 K, **b** pH 8.0, 313 K, determination of kinetic order of swelling; representative plot for **c** Fick's model at pH 8.0, 303 K **d** Schott's model at pH 8.0, 313 K

Table 4 Kinetic parameters and correlation coefficients obtained from Fick's and Schott's models at all pH and all temperatures studied

pH	303 K				313 K			
	Fick's model		Schott's model		Fick's model		Schott's model	
	R^2	k_s (min^{-1})	R^2	k_s (min^{-1})	R^2	k_s (min^{-1})	R^2	k_s (min^{-1})
1.0	0.981	0.031	0.954	−3.27	0.974	0.172	0.995	0.174
3.0	0.993	0.038	0.999	0.035	0.819	0.002	0.896	0.001
5.0	0.992	0.024	0.999	0.025	0.925	0.003	0.931	0.004
7.0	0.964	0.014	0.925	0.016	0.815	0.023	0.197	0.022
8.0	0.973	0.027	0.968	0.030	0.938	0.044	0.943	0.045

$$\frac{t}{W_t} = \frac{1}{k_s W_e^2} + \frac{t}{W_e} \tag{11}$$

The representative graphs of kinetic order of swelling (at 303 and 313 K; pH 8) are shown in Fig. 7c, d. Values of R^2 and swelling rate constant k_s are presented in Table 4. It could be seen from the table that values of correlation coefficient hold good for pseudo-second order at 313 K for all pH values except at pH 7.0, where swelling of the gel follows first-order kinetics. But at 303 K swelling of the gel follows pseudo-second-order kinetics at pH 1.0, 3.0 and 5.0, whereas a transition occurred to first order at pH 7.0 and 8.0.

Network parameters

Due to simplicity of the technique, swelling is widely used to calculate network parameters (polymer volume fraction, molar mass between cross-links, etc.) of cross-linked polymeric materials.

(a) polymer volume fraction ($\nu_{2,s}$) and molecular weight between cross-links (M_c)

Polymer volume fraction is defined as the ratio of the polymer volume (V_p) to the swollen gel volume (V_g). This was used to measure amount of solvent absorbed and retained by the gel and was necessarily calculated (Eq. 12) to predict M_c (molecular weight between cross-links).

$$v_{2,s} = [1 + d_p/d_s(M_a/M_b - 1)]^{-1} \tag{12}$$

Here d_p and d_s are the respective densities of polymer and solvent, while M_a and M_b are the respective masses of hydrogel before and after swelling [39].

One of the significant parameters of cross-linked hydrogels is the molecular weight between neighboring cross-links M_c. Information about the degree of polymer cross-linking was provided by the average value of M_c. Average value of M_c

was used because of the random nature of the polymerization process. Flory–Rehner equation (Eq. 13) was applied to determine M_c of the hydrogel [40, 41]

$$M_c = d_p V_s \left(v_{2,s}^{1/3} - v_{2,s}/2 \right) \left(\ln(1 - v_{2,s}) + v_{2,s} + \chi v_{2,s}^2 \right)^{-1} \quad (13)$$

Here V_s is the molar volume of the swelling agent (in $cm^3\ mol^{-1}$), $v_{2,s}$ is the volume fraction of polymer in the swollen gel, χ is the Flory–Huggins interaction parameter between solvent and polymer, and d_p is density of polymer (in gm L^{-1}) [41].

The volume fraction of WSCR hydrogel decreased with pH, and molecular weight between the cross-links was increased except at pH 7 at 303 K as indicated in Table 5. The overall lower values of M_c suggested that the hydrogel has a compact structure with lower average molecular weight of polymer chains between two adjacent cross-links. Furthermore, this may reflect higher cross-linking density [42]. The values of M_c (Table 5) showed that by increasing temperature the swelling response of hydrogel is also elevated due to which the molecular weight between two cross-links has been increased. In addition to temperature, the increase in pH of the medium also imparted positive impact on swelling percentage of the gel. This will further lead to the increase in molecular weight between adjacent cross-links. So the best swelling activity of WSCR gel was observed at pH 8 and 313 K. Moreover, good correlation of linear regression was found when $v_{2,s}$ and M_c were plotted against equilibrium degree of swelling. Similar results had been obtained by Yarimkaya and Basan [38] while studying the swelling behavior of poly (2-hydroxyethyl methacrylate-co-acrylic acid-co-ammonium acrylate) hydrogels. So, WSCR hydrogel may suitably be used to deliver drug to colon part of gastrointestinal tract of the body (309 K and pH 8).

Table 5 Network parameters and diffusion exponent calculated for WSCR hydrogel at different temperatures and pH

T (K)	pH	Q_e g/g	V_{2s} dm^3	M_c g/mol	Diffusion exponent (n)
303	1.0	0.512	0.609	84.28	0.178
	3.0	3.694	0.999	103	0.996
	5.0	2.825	0.999	144	0.851
	7.0	0.366	0.686	51.17	0.472
	8.0	0.821	0.493	188	0.442
313	1.0	0.673	0.543	131.7	0.885
	3.0	1.528	0.999	139	0.831
	5.0	1.390	0.999	145	0.851
	7.0	0.747	0.517	159	0.928
	8.0	0.880	0.476	214	0.952

Conclusion

FTIR and XRD analyses confirmed the formation of WSCR hydrogel. The synthesized WSCR gel followed three-step thermal degradation, while the first followed complex mechanism as inferred from the master plot method, i.e., A_2 model ($n=2$) for $\alpha=0.1$–0.5. The equilibrium swelling of the gel was maximum at 313 K and pH 8.0 exhibiting stimuli (temperature and pH)-responsive nature. The values of diffusion exponent proposed Fickian behavior at lower temperature and anomalous behavior at higher temperature. The gel followed pseudo-first-order kinetics at lower temperature and pseudo-second order at higher temperature. M_c increased and V_{2s} decreased with the rise of pH. The synthesized gel because of exhibiting best swelling response at pH 8.0 and 313 K may be used as a candidate for controlled drug delivery systems.

References

1. Xavier JR, Thakur T, Desai P, Jaiswal MK, Sears N, Cosgriff-Hernandez E, Kaunas R, Gaharwar AK (2015) Bioactive nanoengineered hydrogels for bone tissue engineering: a growth-factor-free approach. ACS Nano 9:3109–3118. https://doi.org/10.1021/nn507488s
2. Ahmed EM (2015) Hydrogel: preparation, characterization, and applications: a review. J Adv Res 6:105–121. https://doi.org/10.1016/j.jare.2013.07.006
3. Zhou T, Wang Y, Huang S, Zhao Y (2018) Synthesis composite hydrogels from inorganic-organic hybrids based on leftover rice for environment-friendly controlled-release urea fertilizers. Sci Total Environ 615:422–430. https://doi.org/10.1016/j.scitotenv.2017.09.084
4. Zhou G, Luo J, Liu C, Chu L, Ma J, Tang Y, Zeng Z, Luo S (2016) A highly efficient polyampholyte hydrogel sorbent based fixed-bed process for heavy metal removal in actual industrial effluent. Water Res 89:151–160. https://doi.org/10.1016/j.watres.2015.11.053
5. Hu H, Xin JH, Hu H (2014) PAM/graphene/Ag ternary hydrogel: synthesis, characterization and catalytic application. J Mater Chem A 2:11319–11333. https://doi.org/10.1039/C4TA01620C
6. Niranjana PT, Prashantha K (2016) A review on present status and future challenges of starch based polymer films and their composites in food packaging applications. Polym Compos. https://doi.org/10.1002/pc.24236
7. Woo K, Seib PA (1997) Cross-linking of wheat starch and hydroxypropylated wheat starch in alkaline slurry with sodium trimetaphosphate. Carbohydr Polym 33:263–271. https://doi.org/10.1016/S0144-8617(97),00037-4
8. Sulaiman NS, Hashim R, Hiziroglu S, Amini MHM, Sulaiman O, Ezwanselamat M (2016) rubberwood particleboard manufactured using epichlorohydrin-modified rice starch as a binder. Cellul Chem Technol 50:329–338
9. Gui-Jie M, Peng W, Xiang-Sheng M, Xing Z, Tong Z (2006) Crosslinking of corn starch with sodium trimetaphosphate in solid state by microwave irradiation. J Appl Polym Sci 102:5854–5860. https://doi.org/10.1002/app.24947
10. El-Tahlawy K, Venditti RA, Pawlak JJ (2007) Aspects of the preparation of starch microcellular foam particles crosslinked with glutaraldehyde using a solvent exchange technique. Carbohydr Polym 67:319–331. https://doi.org/10.1016/j.carbpol.2006.05.029
11. Singh B, Khurana RK, Garg B, Saini S, Kaur R (2017) Stimuli-responsive systems with diverse drug delivery and biomedical applications: recent updates and mechanistic pathways. Crit Rev Ther Drug Carrier Syst 34. pubmed/28845760
12. Bates FL, French D, Rundle RE (1943) Amylose and amylopectin content of starches determined by their iodine complex formation. J Am Chem Soc 65:142–148. https://doi.org/10.1021/ja01242a003
13. Perez LAB, Agama-Acevedo E (2018) Starch. Starch based Mater Food Packag. https://doi.org/10.1016/B978-0-12-809439-6.00001-7

14. Liang R, Yuan H, Xi G, Zhou Q (2009) Synthesis of wheat straw-g-poly (acrylic acid) superabsorbent composites and release of urea from it. Carbohydr Polym 77:181–187. https://doi.org/10.1016/j.carbpol.2008.12.018
15. Koh JJ, Zhang X, He C (2017) Fully biodegradable poly (lactic acid)/starch blends: a review of toughening strategies. Int J Biol Macromol. https://doi.org/10.1016/j.ijbiomac.2017.12.048
16. Otey FH, Westhoff RP, Russell CR (1976) Starch graft copolymers-degradable fillers for poly (vinyl chloride) plastics. Ind Eng Chem Product Res Dev 15:139–142
17. Morita I et al (1987) Synthesis and antihypertensive activities of 1, 4-dihydropyridine-5-phosphonate derivatives. II. Chem Pharm Bull 35:4144–4154. https://doi.org/10.1248/cpb.35.4144
18. Zhou K, Wang XM, Zhao YZ, Cao YX, Fu Q, Zhang SQ (2011) Synthesis and antihypertensive activity evaluation in spontaneously hypertensive rats of nitrendipine analogues. Med Chem Res 20(8):1325–1330. https://doi.org/10.1007/s00044-010-9477-0
19. Chiang CL, Chang RC, Chiu YC (2007) Thermal stability and degradation kinetics of novel organic/inorganic epoxy hybrid containing nitrogen/silicon/phosphorus by sol–gel method. Thermochim Acta 453:97–104. https://doi.org/10.1016/j.tca.2006.11.013
20. Chiang CL, Ma CCM (2002) Synthesis, characterization and thermal properties of novel epoxy containing silicon and phosphorus nanocomposites by sol–gel method. Eur Polym J 38:2219–2224. https://doi.org/10.1016/S0014-3057(02),00123-4
21. Omrani A, Rostami AA, Sedaghat E (2010) Kinetics of cure for a coating system including DGEBA ($n=0$)/1, 8-NDA and barium carbonate. Thermochim Acta 497:21–26. https://doi.org/10.1016/j.tca.2009.08.004
22. Fanta GF et al (1966) Graft copolymers of starch. I. Copolymerization of gelatinized wheat starch with acrylonitrile. Fractionation of copolymer and effect of solvent on copolymer composition. J. Appl Polym Sci 10(6):929–937. https://doi.org/10.1002/pol.1966.110041018
23. Lanthong P, Nuisin R, Kiatkamjornwong S (2006) Graft copolymerization, characterization, and degradation of cassava starch-g-acrylamide/itaconic acid superabsorbents. Carbohydr Polym 66:229–245. https://doi.org/10.1016/j.carbpol.2006.03.006
24. Wang Y, Zhang L, Li X, Gao W (2011) Physicochemical properties of starches from two different yam (Dioscorea opposita Thunb.) residues. Braz Arch Biol Technol 54:243–251. https://doi.org/10.1590/s1516-89132011000200004
25. Fares MM, El-faqeeh AS, Osman ME (2003) Graft copolymerization onto starch–I. Synthesis and optimization of starch grafted with N-tert-butylacrylamide copolymer and its hydrogels. J Polym Res 10:119–125. https://doi.org/10.1023/A:1024928722345
26. Akbar J, Iqbal MS, Massey S, Masih R (2012) Kinetics and mechanism of thermal degradation of pentose-and hexose-based carbohydrate polymers. Carbohydr Polym 90:1386–1393. https://doi.org/10.1016/j.carbpol.2012.07.008
27. Senum GI, Yang RT (1977) Rational approximations of the integral of the Arrhenius function. J Therm Anal 11:445–447. https://doi.org/10.1007/BF01903696
28. Coats AW, Redfern JP (1964) Kinetic parameters from thermogravimetric data. Nature 201:68. https://doi.org/10.1038/201068a0
29. Vlaev L, Nedelchev N, Gyurova K, Zagorcheva A (2008) A comparative study of non-isothermal kinetics of decomposition of calcium oxalate monohydrate. J Anal Appl Pyrolysis 81:253–262. https://doi.org/10.1016/j.jaap.2007.12.003
30. Bamford CH, Tipper CFH, Compton RG (1986) Electrode kinetics: principles and methodology, vol 26. Elsevier, Amsterdam
31. Georgieva V, Zvezdova D, Vlaev L (2013) Non-isothermal kinetics of thermal degradation of chitin. J Therm Anal Calorim 111:763–771. https://doi.org/10.1007/s10973-012-2359-6
32. Liu J, Li Q, Su Y, Yue Q, Gao B (2014) Characterization and swelling–deswelling properties of wheat straw cellulose based semi-IPNs hydrogel. Carbohydr Polym 107:232–240. https://doi.org/10.1016/j.carbpol.2014.02.073
33. Hiremath JN, Vishalakshi B (2012) Effect of crosslinking on swelling behaviour of IPN hydrogels of Guar Gum and Polyacrylamide. Der Pharma Chem 4: 946–955. ISSN 0975-413X
34. Anirudhan TS, Parvathy J (2014) Novel semi-IPN based on crosslinked carboxymethyl starch and clay for the in vitro release of theophylline. Inter J Biol Macromol 67:238–245. https://doi.org/10.1016/j.ijbiomac.2014.03.041
35. Peppas NA, Bures P, Leobandung W, Ichikawa H (2000) Hydrogels in pharmaceutical formulations. Eur J Pharm Biopharm 50:27–46. https://doi.org/10.1016/S0939-6411(00),00090-4

36. Karadag E, Saraydin D (1995) Swelling of acrylamide-tartaric acid hydrogels. Iran J Polym, Sci Technol, p 4
37. Ritger PL, Peppas NA (1987) A simple equation for description of solute release II. Fickian and anomalous release from swellable devices. J Control Release 5:37–42. https://doi.org/10.1016/0168-3659(87),90035-6
38. Yarimkaya S, Basan H (2007) Swelling behavior of poly (2-hydroxyethyl methacrylate-co-acrylic acid-co-ammonium acrylate) hydrogels. J Macromol Sci Part A Pure Appl Chem 44:939–946. https://doi.org/10.1080/10601320701424198
39. Ding ZY, Aklonis JJ, Salovey R (1991) Model filled polymers. VI. Determination of the crosslink density of polymeric beads by swelling. J Polym Sci Part B Polym Phys 29:1035–1038. https://doi.org/10.1002/polb.1991.090290815
40. Flory PJ, Rehner JJ (1943) Statistical mechanics of cross-linked polymer networks II. Swelling. J Chem Phys 11:512–520. https://doi.org/10.1063/1.1723792
41. Sohail K, Khan IU, Shahzad Y, Hussain T, Ranjha NM (2014) pH-sensitive polyvinylpyrrolidone-acrylic acid hydrogels: impact of material parameters on swelling and drug release. Braz J Pharm Sci 50(1):173–184. https://doi.org/10.1590/s1984-82502011000100018
42. Wong RSH, Ashton M, Dodou K (2015) Effect of crosslinking agent concentration on the properties of unmedicated hydrogels. Pharmaceutics 7(3):305–319. https://doi.org/10.3390/pharmaceutics7030305